A study of the magnetic and electrical crossover region of $La^{0.5\pm\delta}Ca^{0.5\mp\delta}MnO_3$

1999 J. Phys.: Condens. Matter 11 4843

(http://iopscience.iop.org/0953-8984/11/25/305)

J. Phys.: Condens. Matter **11** (1999) 4843–4859. Printed in the UK PII: S0953-8984(99)00466-X

A study of the magnetic and electrical crossover region of $La_{0.5\pm\delta}Ca_{0.5\mp\delta}MnO_3$

M Roy†, J F Mitchell‡, A P Ramirez§ and P Schiffer†

† Department of Physics, University of Notre Dame, IN 46556, USA
‡ Material Science Division, Argonne National Laboratory, Argonne, IL 60439, USA
§ Lucent Technologies, Bell Laboratory, Murray Hill, NJ 07974, USA

E-mail: schiffer.1@nd.edu

Received 30 December 1998

Abstract. The ground states of $La_{1-x}Ca_xMnO_3$ change from double-exchange-associated conducting ferromagnets at $x < 0.50$ to charge-ordered antiferromagnets at $x > 0.50$ even when x is varied only slightly around 0.50. We have performed a careful study of the electrical and magnetic properties of these materials for a range of samples with slightly varying calcium doping around $x \approx 0.50$. The natures of the ground state and the transition were found to be sensitive not only to the calcium doping but also to the actual Mn^{4+} content of these materials. The low-temperature resistivity of the $x \approx 0.50$ materials below the charge-ordering temperature was found to drop with decreasing temperature in the presence of magnetic fields of even a few teslas or a slight Ca underdoping ($x \lesssim 0.50$), revealing the presence of some free carriers even in the charge-ordered states. The data therefore demonstrate a coexistence of ferromagnetic conducting and antiferromagnetic charge-ordered phases in the perovskite manganites. We also observe field-induced 'annealing' in the charge-ordered state due to the partial delocalization of the carriers.

1. Introduction

The intricate interplay of the magnetic and transport properties of $R_{1-x}Ae_xMnO_3$ (where R^{3+} is a rare earth and Ae^{2+} is a Ca, Sr, Ba, etc) has generated much recent interest [1]. The properties of these materials are extremely sensitive to temperature, external magnetic and electric fields, doping, applied pressure, and the ionic radii of both the trivalent and divalent ions [2, 3]. Among these materials [4–7], $La_{1-x}Ca_xMnO_3$ is particularly interesting, since it can be prepared over the whole range of doping ($0 \leqslant x \leqslant 1$). In the low-doping or colossal-magnetoresistance (CMR) regime ($0.2 < x < 0.4$), it exhibits a large magnetoresistance associated with a ferromagnetic transition. This behaviour is qualitatively explained by double-exchange (DE) theory [8], where the ferromagnetic transition is mediated by the e_g electron between the aligned Mn^{4+} core spins. Despite the great success of the DE theory in explaining these features qualitatively, it cannot quantitatively fit the experimental data, and it has been recently recognized that the electron–phonon coupling associated with the Jahn–Teller (JT) distortion of the $Mn^{3+}O_6$ octahedra also plays an important role in these materials [9]. In the higher-doping regime ($x \gtrsim 0.50$), the charges become localized due to Coulomb and electron–phonon interactions, creating a charge ordering of the localized e_g electrons in the periodic crystalline lattice of the spatially ordered Mn^{3+} and Mn^{4+} ions. The charge ordering of the Mn^{3+} and Mn^{4+} ions in turn suppresses the DE-induced ferromagnetic (FM) interactions, and

0953-8984/99/254843+17$19.50

at a lower temperature the spins order into a superexchange-induced antiferromagnetic (AFM) state [10, 11].

The properties of these materials in the intermediate-doping regime ($x \approx 0.50$), where the system undergoes a doping-dependent metal–insulator transition (MIT), are quite different from both those of the ferromagnetic conducting regime and those of the charge-ordering regime [7, 10]. The properties at $x \sim 0.50$ change a great deal when x is varied only slightly, because the ground state ranges from a FM metallic state at low doping ($x \lesssim 0.45$) to a fully charge-ordered AFM insulating state at high doping ($x \gtrsim 0.55$). In the intermediate regime ($x \sim 0.50$), there is a competition between the e_g electron-mediated FM double exchange and the JT-induced charge ordering. The materials in the intermediate-doping regime exhibit traces of both states, since the energy scales of these two interactions are quite comparable in this regime. At high temperatures, due to the thermal fluctuations, they behave like paramagnetic insulators. But at lower temperatures, they undergo a transition first to ferromagnetic spin ordering and then to a charge-ordered state with high resistivity, and finally to an antiferromagnetic spin state. The charge-ordered state is quite unusual in this doping regime as it can be dissociated or 'melted' by an applied magnetic field [12–17].

Even though $La_{1-x}Ca_xMnO_3$ is a widely studied material, most of the research has been concentrated in the low-doping or fully charge-ordered regime. We have performed a detailed study of the doping-induced MIT through the crossover region, by studying a number of samples closely spaced in doping with $x \approx 0.50$ and with well characterized Mn^{4+} content. We found that the materials in this regime are very sensitive to both x and the actual Mn^{4+} content, and that their properties differ a great deal when either of them is varied only slightly. We model the electrical behaviour of these samples as being due to the existence of free carriers in the charge-ordered state. We also observe field-induced 'annealing' in the charge-ordered state due to the partial delocalization of the carriers. A preliminary report of some of the data has been published previously [18].

2. Experimental details

Samples of $La_{1-x}Ca_xMnO_3$ with Mn^{4+} and Ca concentrations as listed in table 1 were prepared by combining stoichiometric quantities of La_2O_3, $CaCO_3$, and MnO_2 and then calcining at 1000 °C. The powder was subsequently fired at 1250 °C and 1350 °C with intermediate grindings and then pressed into pellets and fired at 1400 °C in flowing oxygen; this was followed by slow cooling at room temperature. The resulting black pellets were all single phase as adjudged by powder x-ray diffraction. We determined the Mn^{4+} content within

Table 1. List of samples.

Sample number	Ca content	Mn^{4+} content (%)
1	0.33	37.2
2	0.42	34.8
3	0.48	49.0
4	0.48	53.2
5	0.49	52.8
6	0.50	53.8
7	0.51	53.6
8	0.52	49.2
9	0.52	55.2
10	0.55	58.2

1% for each sample by redox titration, with the precision determined by running several (typically 5–10) separate runs on each sample. As a measure of the accuracy of the method, a sample of $La_{0.79}Ca_{0.21}MnO_{3.1555}$ ($\delta = 0.155$, determined by thermogravimetric analysis) was analysed. The redox titration gave a value of $Mn^{4+} = 52.8\%$, equivalent to $\delta = 0.159$. The differences between the content of Mn^{4+} and x probably arise from small ($\lesssim 1\%$) oxygen off-stoichiometries. The resistivity was measured by the standard ac four-probe in-line method and the dc magnetization was measured by a commercial SQUID magnetometer.

3. Temperature-dependent studies

3.1. Data

Figures 1 and 2 show the resistivity and magnetization of the measured samples on warming and cooling. The samples (see table 1) can be divided into three broad doping regimes.

3.1.1. The low-doping regime. The resistivity and the magnetization of samples 1 and 2, with $x = 0.33$ and 0.42, show behaviour typical of the CMR regime in which the ground state is a FM conductor. The samples display a FM transition at $T \sim 270$ K with an accompanying drop in $\rho(T)$. The magnetization reaches >80% saturation at low temperature and magnetic fields greater than 1 T. Moreover, $\rho(T)$ near the FM transition temperature (T_c) is suppressed greatly in the presence of an external magnetic field of even a few teslas, and as a result displays a large magnetoresistance.

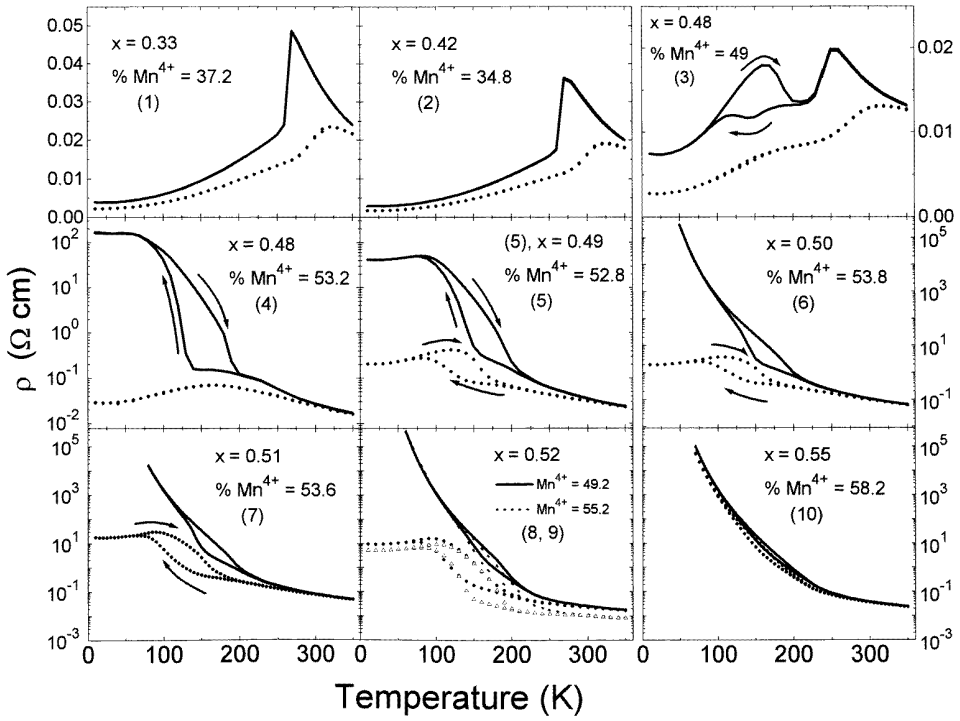

Figure 1. The temperature-dependent resistivity at $H = 0$ T (solid curves) and $H = 6$ T (solid circles) on warming and cooling. The corresponding sample number is shown in parentheses.

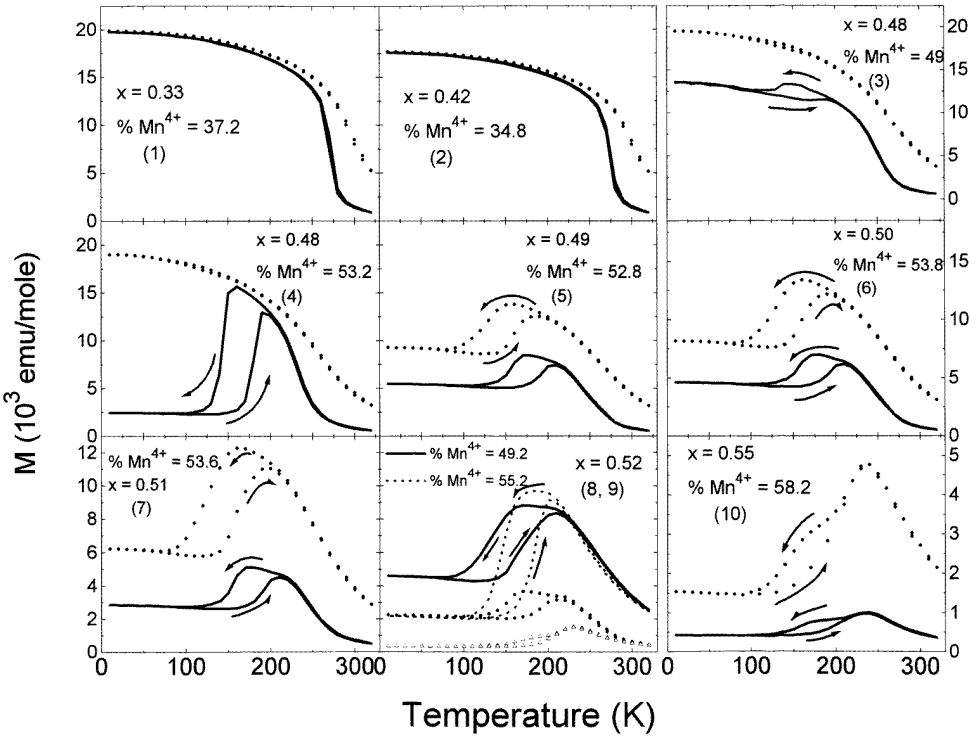

Figure 2. The temperature-dependent magnetization at $H = 1$ T (solid curves) and $H = 6$ T (solid circles) on warming and cooling. The corresponding sample number is shown in parentheses.

3.1.2. The intermediate-doping regime. The resistivity data from samples $3 \rightarrow 9$ (see table 1) at low fields show the effects of charge ordering. On cooling at low fields the magnetization of the these samples shows a FM transition, but at lower temperature it drops sharply with a corresponding rise in $\rho(T)$ due to the charge ordering of the Mn^{4+} and Mn^{3+} ions. Moreover, both $\rho(T)$ and $M(T)$ exhibit strong hysteresis, indicating the first-order nature of this transition. In a moderate applied magnetic field, however, $\rho(T)$ is suppressed greatly, displaying a large magnetoresistance. Since the properties of these samples vary greatly, we discuss each in detail.

(a) *Sample 3.* The sample with $x = 0.48$ ($Mn^{4+} = 49\%$) demonstrates characteristics of both the low- and the intermediate-doping regime. At $H = 0$ the resistivity displays a sharp drop on cooling at $T \sim 250$ K with an accompanying FM transition. At a lower temperature ($T \sim 180$ K) $M(T)$ drops slightly, a feature which exhibits some hysteresis on warming in low fields. In fact, at the same temperature, $\rho(T)$ also appears to rise slightly on cooling before finally dropping to 50% of its peak value as $T \rightarrow 0$. But more interestingly, on warming it displays an additional peak at $T \sim 160$ K and as a result shows a very strong hysteresis. We believe that these features are due to the reduction in FM double exchange associated with the onset of charge ordering. The second peak in $\rho(T)$ and the hysteresis in $\rho(T)$ and $M(T)$ disappear at $H \gtrsim 5$ T with $M(T)$ reaching $>80\%$ of its full FM saturation at low temperatures.

(b) *Samples 4 and 5.* Both samples show the typical characteristics of the intermediate regime at low fields. Although $\rho(T)$ at low fields rises sharply with an accompanying

drop in $M(T)$ at the charge-ordering temperature (T_{co}), $\rho(T)$ subsequently drops at a lower temperature (this will be discussed in detail later in the text). Moreover, a large magnetoresistance is observed at $H \gtrsim 0.5$ T. Although samples 4 and 5 qualitatively behave in a similar fashion at low fields, they behave rather differently at moderate fields ($H > 5$ T). While sample 5 undergoes a first-order FM $\rightarrow$ charge-ordered transition demonstrated by the sharp rise and hysteresis in $\rho(T)$ and a sudden drop in $M(T)$ even at $H \sim 9$ T, sample 4 displays all of the characteristics of the low-doping regime at $H \gtrsim 5$ T (at high fields both $M(T)$ and $\rho(T)$ for sample 4 show no hysteresis and $M(T)$ reaches >80% FM saturation).

(c) *Samples* $6 \rightarrow 9$. At $H \lesssim 3$ T, $\rho(T)$ rises steeply due to the charge ordering for all $T < T_{co}$, but at a higher field, $\rho(T)$ decreases with temperature at temperatures well below the charge-ordering temperature. Both $\rho(T)$ and $M(T)$ remain strongly hysteretic even in high fields ($H = 9$ and 7 T respectively), suggesting that the charge lattice does not quite dissociate even at $H \sim 9$ T, which is further demonstrated by the rather high resistivity of these samples ($\rho > 0.1\ \Omega$ cm). Samples $6 \rightarrow 8$ exhibit a high moment (in the FM temperature regime); however, $M(T)$ reaches less than 50% of their ferromagnetic saturations even at $H \sim 7$ T. Although sample 9 qualitatively behaves like samples $6 \rightarrow 8$, $M(T)$ for $0.5 \lesssim H \lesssim 5$ T displays a distinctive second feature on cooling which is also observed for sample 10 as is discussed below.

3.1.3. The high-doping regime. At $x = 0.55$, $\rho(T)$ is activated down to the lowest temperatures. Even at $H \sim 9$ T, $\rho(T)$ displays little hysteresis and effectively no magnetoresistance, suggesting that the sample remains mainly charge ordered even at $H \sim 9$ T. The magnetization, however, exhibits a large hysteresis. On warming it drops sharply at $T \sim 210$ K due to the onset of charge ordering. But on cooling, in addition to the charge-ordering drop for $H \gtrsim 0.5$ T, $M(T)$ displays a distinctive second feature at a lower temperature, T_M (the slope of $M(T)$ decreases at $T \sim T_M$ before a subsequent drop). At low fields ($H \lesssim 0.5$ T), however, $M(T)$ behaves qualitatively like the lower-doping materials (samples $6 \rightarrow 8$). We believe that this behaviour is due to the presence of FM regions in a largely CO sample, and that these FM regions undergo a first-order phase transition to a charge-ordered state at a lower temperature than the bulk of the sample. Moreover, while T_M decreases by ~20 K between 0 and 7 T with increasing field as illustrated in the inset to figure 3(a), T_{co} (as indicated by a sharp drop in $M(T)$) changes only by ~5 K with the field, suggesting that the bulk of the material remains charge ordered even at high fields.

3.2. Discussion

3.2.1. The temperature-dependent phase transition. The charge ordering in these materials is demonstrated by a sharp rise in $\rho(T)$ with a corresponding drop in $M(T)$. We find that T_{co} for samples $4 \rightarrow 9$ changes by ~50 K between warming and cooling, demonstrating the first-order nature of this transition. The magnetic field delocalizes the e_g electrons, and as a result T_{co} decreases monotonically with field, as is illustrated in figure 3(b). The charge-ordering temperature (T_{co}) also increases monotonically with the Ca content and the actual Mn^{4+} content (see figure 3(b)), demonstrating the localization of the JT distortion as the Ca/Mn^{4+} content increases from 50%. This is further demonstrated by the much smaller moment and the apparent absence of a bulk FM state in the samples with higher Mn^{4+} doping ($x = 0.52$ ($Mn^{4+} = 55.2\%$) and $x = 0.55$ ($Mn^{4+} = 58.2\%$)).

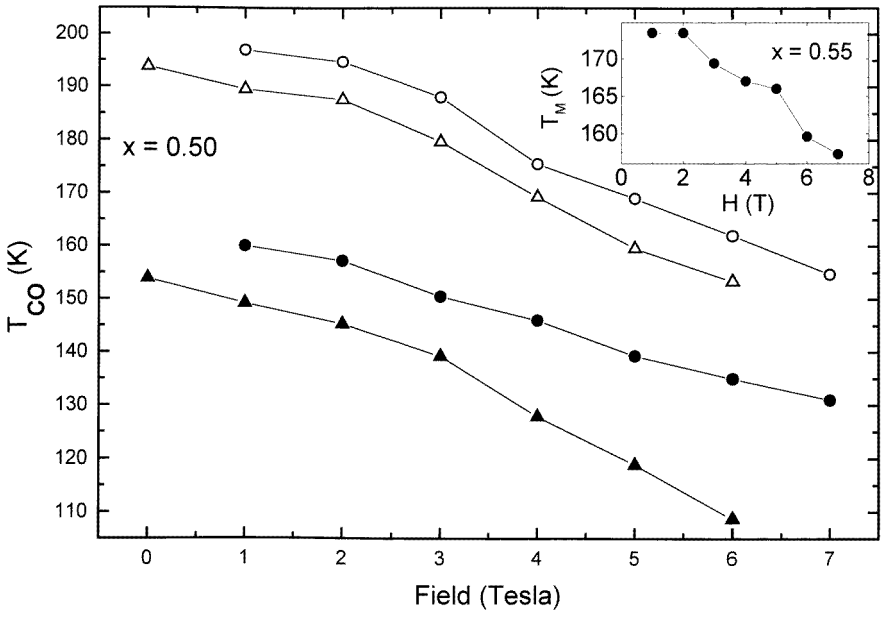

(a)

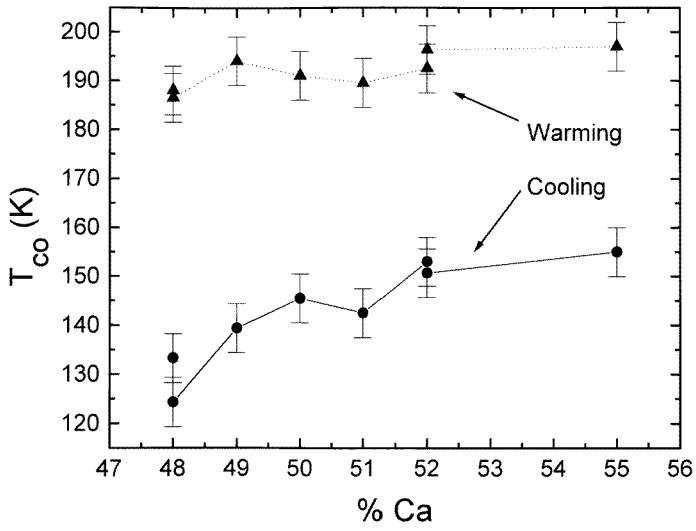

(b)

Figure 3. (a) The charge-ordering temperature (T_{co}) as a function of field, for sample 6 ($x = 0.50$ ($Mn^{4+} = 53.8\%$)) on warming and cooling, obtained from the extremum of $d(\ln \rho)/dT$ on cooling (closed triangles) and on warming (open triangles), and dM/dT on cooling (closed circles) and on warming (open circles) The inset illustrates the lower transition temperature (T_M) upon cooling of sample 10 ($x = 0.55$ ($Mn^{4+} = 58.2\%$)) as a function of field. (b) The charge-ordering temperature (T_{co}) as a function of doping on warming (triangles) and cooling (circles) at $H = 0$ T, calculated from the peak of $d(\ln \rho)/dT$.

3.2.2. The importance of both the Ca content and the Mn^{4+} content. The importance of both the Ca content and the actual Mn^{4+} content in the intermediate-doping regime is clearly

demonstrated in figure 4. There are two pairs of samples with the same Ca doping, samples 3 and 4 with $x = 0.48$ ($Mn^{4+} = 49\%$ and 53.2%) and samples 8 and 9 with $x = 0.52$ ($Mn^{4+} = 49.2\%$ and 55.2%). The behaviour of sample 3, with $x = 0.48$ ($Mn^{4+} = 49\%$), is closely related to that of the low-doping regime in that the ground state is FM conducting. The resistivity first displays a peak at the ferromagnetic T_c and then drops sharply on cooling as in the low-doping regime. But on warming it shows an additional maximum associated with charge ordering, displaying a strong hysteresis. The disappearance of this second peak in ρ and the fact that $M(T)$ reaches its full ferromagnetic saturation at $H \gtrsim 5$ T suggest that the charge-ordered state completely dissociates at high fields. The behaviour of sample 4 is quite different. The zero-field ground state of this sample has high resistivity, and the suppression of the e_g electron-mediated ferromagnetism is further displayed by the sharp drop in magnetization at low fields. But it is interesting to note that unlike the case for samples $5 \rightarrow 9$, both $\rho(T)$ and $M(T)$ indicate a ferromagnetic state with high conductivity at low temperatures and high fields ($H \gtrsim 5$ T). Although the sample properties cannot be determined by x, the Mn^{4+} content alone also cannot determine the properties of these materials. This is

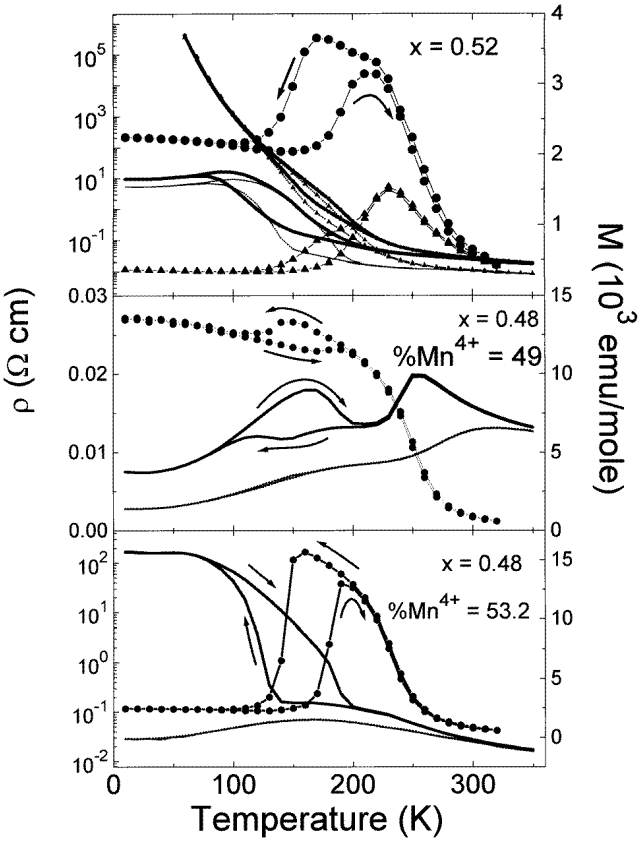

Figure 4. An enlarged view of the temperature-dependent magnetization and resistivity of the two pairs of samples with the same Ca content but different Mn^{4+} contents (as discussed in the text, demonstrating the importance of both x and Mn^{4+}). The bottom two panels show $\rho(T)$ at $H = 0$ T (solid curves) and $H = 6$ T (dotted curves) and $M(T)$ at $H = 1$ T. The top panel shows $\rho(T)$ at $H = 0$ T and 6 T for $x = 0.52$ and $Mn^{4+} = 49.2\%$ (solid curves) and 55.2% (dotted curves) and $M(T)$ for the same samples at $H = 1$ T, for $Mn^{4+} = 49.2\%$ (triangles) and 55.2% (circles).

evident from samples 8 and 9 with $x = 52$ for which $\rho(T)$ is similar both qualitatively and quantitatively even though the Mn^{4+} content is quite different. The effect of the Mn^{4+} content is, however, evident in $M(T)$, which is quite different for this pair of samples. Sample 8 with $Mn^{4+} = 49.2\%$ has a magnetization $M(T)$ which is qualitatively similar to those of samples $4 \rightarrow 7$ with smaller x. Its ferromagnetic transition temperature ($T_c \sim 243$ K) is close to that of the samples with $x \approx 0.50$. By contrast, $M(T)$ for $Mn^{4+} = 55.2\%$ qualitatively resembles that of the higher-doping regime, and T_c is also significantly lower than for sample 8.

The importance of both the Ca content and the actual Mn^{4+} content is further illustrated in figure 5, which shows the variation of the low-temperature resistivity and magnetization across the doping-dependent metal–insulator transition (MIT). The doping-dependent MIT is sensitive to both the Ca content and the actual Mn^{4+} content (as is illustrated in figure 5), occurring at $x \sim 0.49$ but at $Mn^{4+} \sim 53\%$. This represents a significant difference, since the transition width is only ~1%. This difference and the presence of two outlying points in the plots very strongly suggest that both the Ca content and the actual Mn^{4+} content are important in determining the properties of these materials in the intermediate regime.

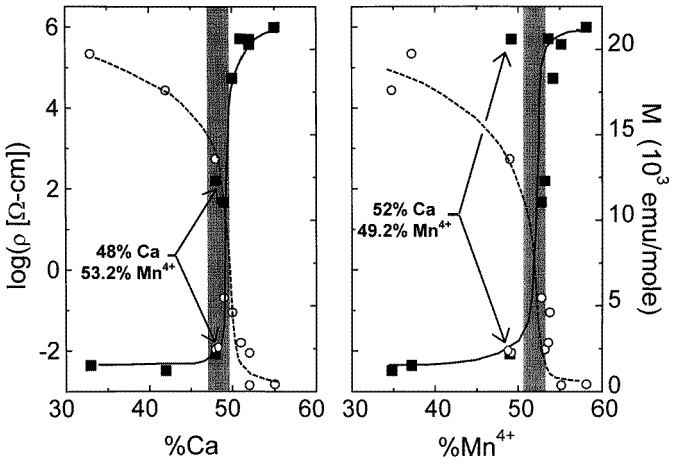

Figure 5. The metal–insulator transition as a function of Ca and Mn^{4+} contents as observed through ρ ($T = 60$ K, $H = 0$ T) (solid squares) and M ($T = 10$ K, $H = 1$ T) (open circles). The curves are guides to the eye and the arrows indicate the samples which are inconsistent with the general trends as discussed in the text. The shaded regions give an estimated maximum range for the MIT based on the precision of our knowledge of the Mn^{4+} and Ca contents and the slope of the data. Reprinted from [18].

3.2.3. Low-temperature behaviour. At low temperatures, samples $4 \rightarrow 9$ show very large magnetoresistances in the presence of magnetic fields of even a few teslas. This large magnetoresistance has been explained as the dissociation or 'melting' of the charge lattice due to the enhancement of double exchange with a field leading to the delocalization of the e_g electrons. In addition to the large magnetoresistance, $\rho(T)$ reaches a maximum at a temperature well below the charge-ordering temperature and subsequently drops with decreasing temperature as $T \rightarrow 0$. This feature is shown by all of the samples with $x > 0.50$ in sufficiently high fields (except for $x = 0.55$) and by samples 3, 4, and 5 even at $H = 0$. As can be seen in figure 6, the extent of this decrease and the temperature range increase with applied field or lower Ca doping. This behaviour is particularly interesting as it suggests the onset of some metallic behaviour

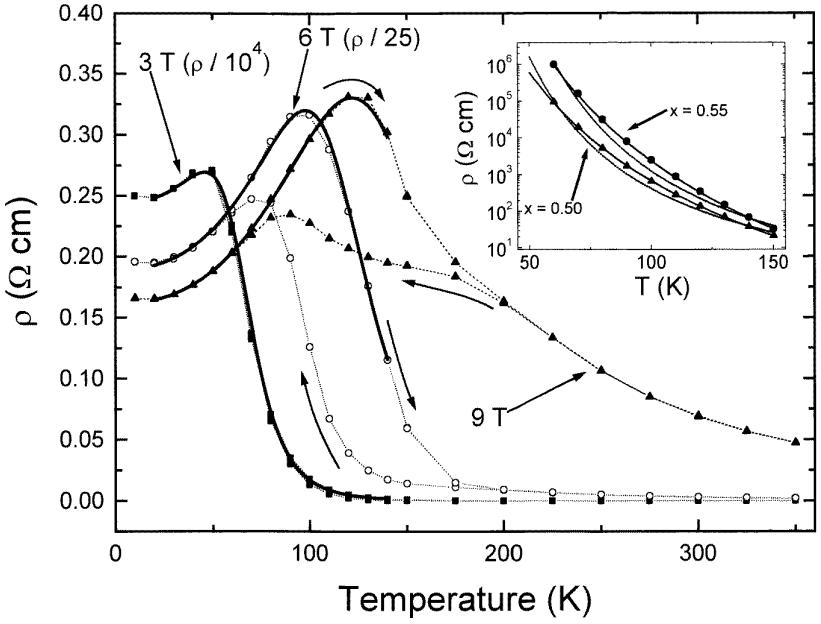

(a)

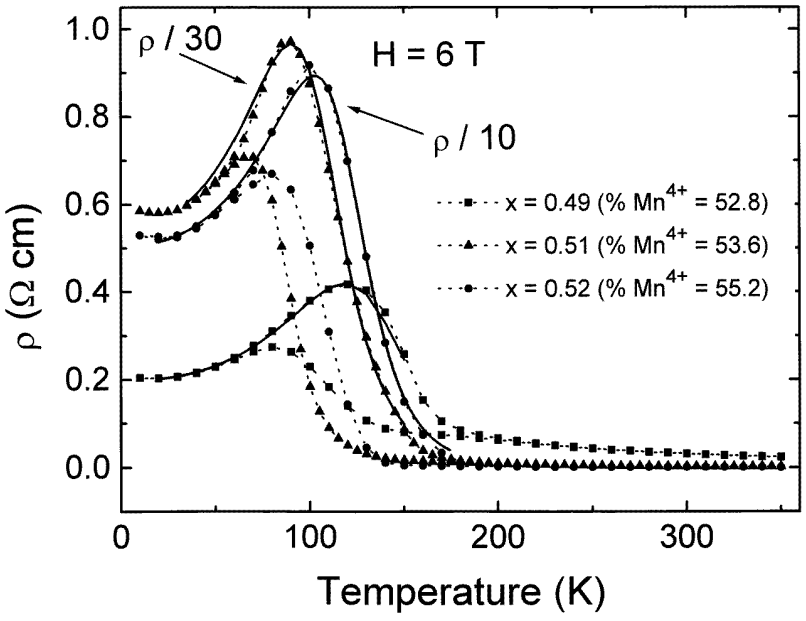

(b)

Figure 6. (a) A linear-scale plot of $\rho(T)$ for $x = 0.50$ at $H = 3$ T (solid squares), $H = 6$ T (open circles), $H = 9$ T (solid triangles) (data at 3 T are divided by a factor of 10 000 and data at 6 T by a factor of 25). The inset illustrates the best fit to low-temperature $\rho(T)$ at $H = 0$ T with the simple activated form $\rho = C\exp[D/T]$ (dashed curves) and the variable-range-hopping form $\rho = C\exp[(D/T)^{1/4}]$ (solid curves) for $x = 0.50$ and 0.55. (b) A linear-scale plot of $\rho(T)$ at $H = 6$ T for $x = 0.49$ (solid squares), 0.50 (solid circles), 0.51 (solid triangles) (data at $x = 0.50$ are divided by a factor of 10 and data at $x = 0.51$ by a factor of 30). The solid curves are fits to the data as discussed in the text.

even in the charge-ordered AFM state, and can also be observed in previously published data, including some taken for high-quality single crystals [14, 19, 20].

We attempt to model this behaviour with a form of $\rho(T)$ based on the coexistence of a small population of free carriers in the charge-ordered state. Such a coexistence is very clearly demonstrated by the presence of two peaks in $\rho(T)$ at low fields for sample 3. In fact, at $H = 9$ T even the sample with $x = 0.50$ displays a second feature on cooling at a higher temperature (see figure 6(a)) associated with the FM transition. We assume the total conductivity below T_{co} to be due to the parallel conduction through activated hopping [21] of excitations in the charge lattice ($\sigma = C \exp -(D/T)^{1/4}$) and by a small population of free carriers ($\rho = A + BT^{2.5}$) where A and B correspond to scattering by defects, and by a combination of phonons, electrons, and spin fluctuations and the exponent of 2.5 is an empirical fit [7]. In this form, ρ can be written as

$$1/\rho = 1/(A + BT^{2.5}) + C \exp -(D/T)^{1/4}. \tag{1}$$

We chose the conduction in the charge lattice to be by variable-range hopping ($\sigma = C \exp -(D/T)^{1/4}$) instead of simple activated conduction ($\sigma = C \exp(-D/T)$, as a simple activated form does not fit the data as well as the variable-range-hopping form (see the inset to figure 6(a)). The above equation fits our data rather well for different values of x as well as at different fields as illustrated in figure 6.

We can analyse the results of the fits at different fields by considering A and B within the structure of a simple Drude model in which we expect

$$1/\rho \propto 1/n\tau \tag{2}$$

where τ is the scattering time, and n is the number of free carriers. On the basis of this model we expect the temperature-dependent and temperature-independent scattering coefficients to be inversely proportional to the number of free carriers and the scattering time. Both $A(H)$ and $B(H)$ change by orders of magnitude with the field (see figure 7(a)) even though the quotient A/B remains independent of the field. The temperature-independent scattering centres are independent of the field, implying that $A(H)$ depends on the field only through the number of free carriers, and therefore the number of free carriers is very strongly field dependent. Moreover, empirically $A(H) \propto B(H)$, suggesting that $B(H)$ also depends on the external magnetic field only through the number of carriers. The facts that $A(H) \propto B(H)$ and both decrease with increasing field (see figure 7(a)) suggest that the large magnetoresistance is due to the increase in the number of carriers rather than the decrease in scattering.

Since τ appears to be largely field independent, we can make a rough estimate of how the carrier density varies with the external field. If we assume that the sample with $x = 0.42$ has $\approx$0.42 carriers/formula unit, we can estimate the field-independent scattering time τ associated with B to obtain an approximate number density of the sample with $x = 0.50$. A plot of this approximate number density $n(H)$ (see the inset to figure 7(a)) illustrates that even at $H \sim 9$ T, $n(H)$ only reaches $\sim$1% of its maximum value, indicating that the charge lattice remains largely intact.

The charge lattice orders more effectively as x and the Mn^{4+} content increase. Since the localization of the JT distortion suppresses the number of free carriers, both of the scattering coefficients A and B are [22] expected to increase with x and Mn^{4+}, and indeed this is the case (see figure 8). The variable-range-hopping parameters C and D [22] characterize the localization of the (charge-ordered) carriers [23]. Figures 7(b) and 8 show the fit parameters C and D as functions of field and doping. These figures suggest that the charge lattice delocalizes in the presence of either external fields or slight Ca or Mn^{4+} underdoping near $x \approx 0.50$.

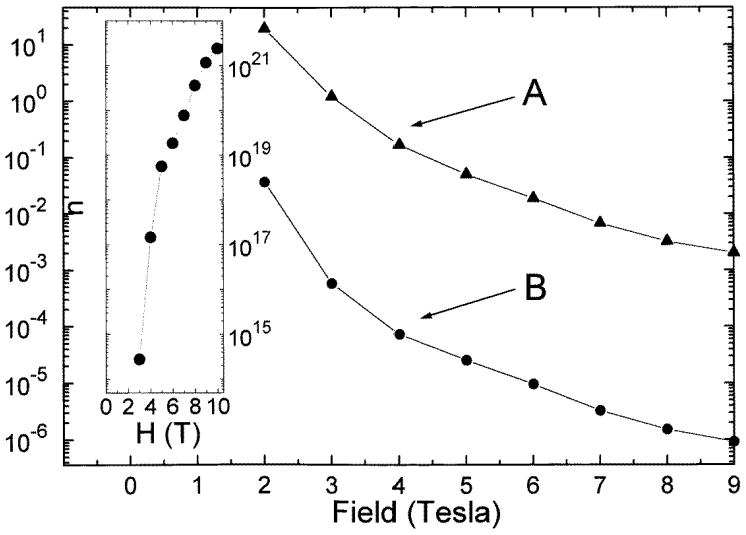

(a)

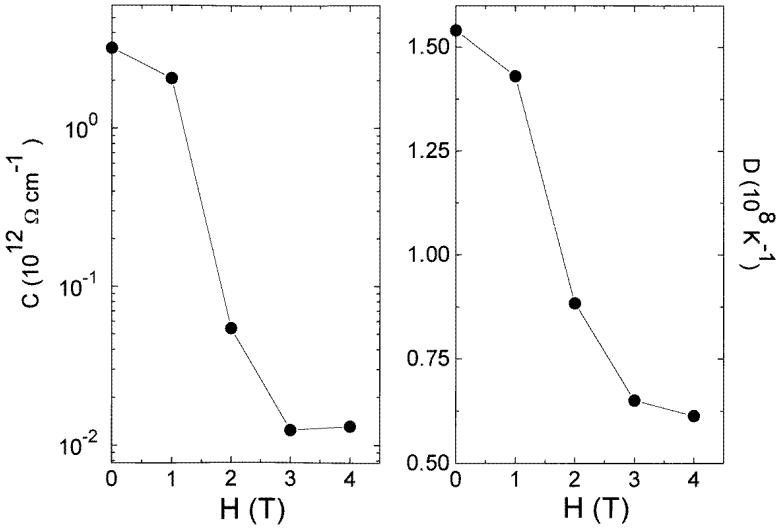

(b)

Figure 7. (a) The fit parameters A (Ω cm) and B (Ω cm $K^{-2.5}$) as functions of field. The inset shows the approximate number density per molar volume of free carriers for $x = 0.50$ as discussed in the text. (b) The fit parameters C and D as functions of field.

4. Field-dependent studies

The rare-earth manganites are known to show unusual behaviour when the applied magnetic field is swept [1, 12, 19, 24–26], and the results for our samples are shown in figure 9. The samples were zero-field cooled (ZFC) to the prescribed temperature, and then $\rho(T, H)$ and $M(T, H)$ were measured in a sweeping field ($0 \rightarrow H_{max}$, $H_{max} \rightarrow -H_{max}$, $-H_{max} \rightarrow H_{max}$), where $H_{max} = 9$ T and 7 T respectively.

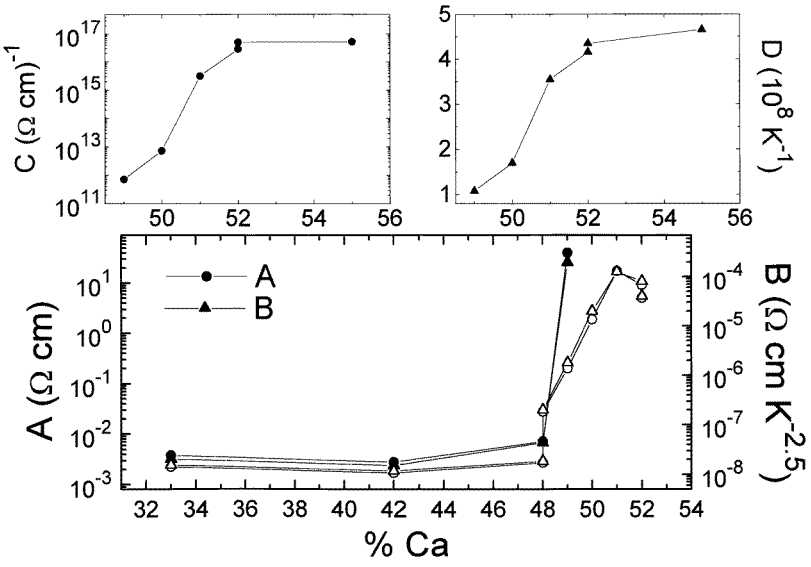

Figure 8. The fit parameters as functions of doping, at $H = 0$ T (closed symbols) and $H = 6$ T (open symbols).

The samples in the lower-doping regime (samples 1 and 2) show the distinctive features of the CMR regime. At low temperatures ($T \ll T_c$), the magnetization increases very sharply with an accompanying sharp drop in $\rho(H)$ at low fields, $H \lesssim H_k$ (the slope of $M(H)$ changes abruptly at $H \sim H_k$). However, at higher fields, $\rho(H)$ decreases gradually with increasing field and $M(H)$ reaches >80% of its full FM saturation. This behaviour has been observed previously for polycrystalline samples of other low-doping manganites [7, 24, 26], and it is associated with grain boundary or domain wall scattering.

At low temperatures (i.e. $T = 5$ K), where the conduction is mostly by the free carriers, sample 3 shows the characteristics of the low-doping regime when the field is swept for the first time. The magnetization increases sharply at low fields ($H < H_k$) with an accompanying sharp drop in ρ. On decreasing the field, even though ρ increases, it never reaches the magnitude of the initial sweep and the resistivity during the subsequent field sweeps does not display any hysteresis. At intermediate temperatures (i.e. $T = 77$ K), both the resistivity and the magnetization display some hysteresis; however, they exhibit no difference between the initial sweep and the subsequent field sweep from $0 \rightarrow 9$ T after a complete magnetic field loop. At high temperatures ($T < T_{co}$), where the charge lattice is largely dissociated, neither $\rho(H)$ nor $M(H)$ exhibits any hysteresis, and in fact both $\rho(H)$ and $M(H)$ qualitatively display the features of the high-temperature ($T > T_c$) characteristics of the samples in the low-doping regime.

Both the resistivity and the magnetization of the samples $4 \rightarrow 9$ show features which are distinct from those of the lower- or higher-doping regimes. At low temperature ($T \lesssim 70$ K, depending on the sample), these materials appear to undergo a MIT at $H \sim H_{MI}$. This is demonstrated by the sharp drop in ρ at $H < H_{MI}$ accompanied by a sharp rise in the magnetization (see figure 9(b). However, at $H > H_{MI}$ the change in $\rho(H)$ and $M(H)$ is much more gradual. While the magnetization during the subsequent field sweeps remains unchanged, ρ remains orders of magnitude lower than for the initial sweep. This suggests that the once the electrons are delocalized by an external magnetic field, they remain mostly delocalized even

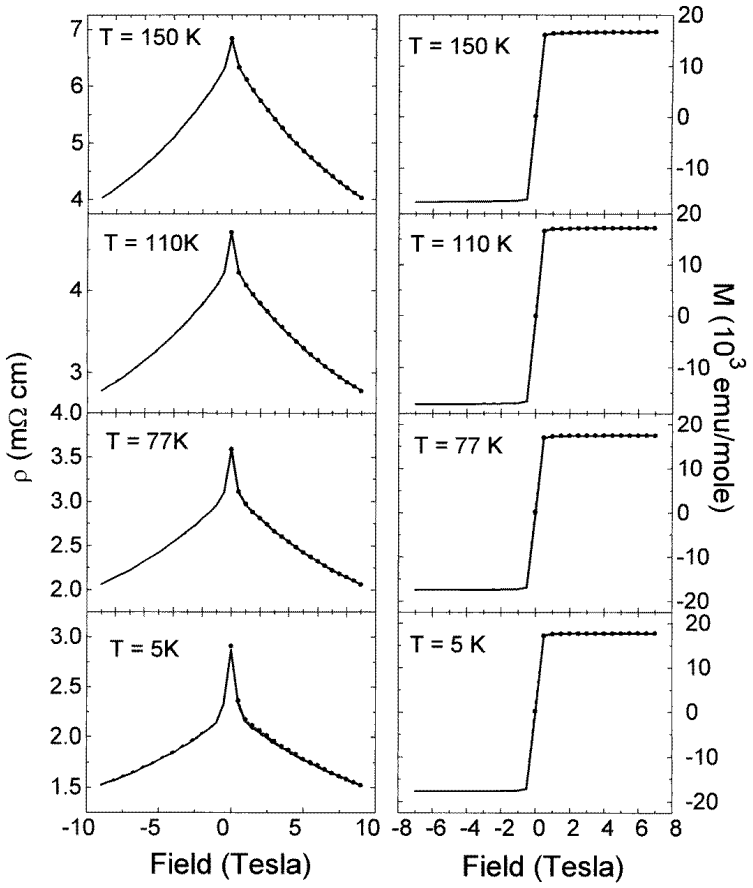

(a)

Figure 9. The resistivity and magnetization at different temperatures upon sweeping the field. The samples were all zero-field cooled, then the field was swept from $0 \rightarrow H_{max}$ (solid circles and curves), $H_{max} \rightarrow 0 \rightarrow -H_{max}$ (dotted curves), and $-H_{max} \rightarrow 0 \rightarrow H_{max}$ (solid curves), where $H_{max} = 9$ T for $\rho(T, H)$ and 7 T for $M(T, H)$; (a) sample 1, $x = 0.42$ ($Mn^{4+} = 34.8\%$), (b) sample 5, $x = 0.49$ ($Mn^{4+} = 52.8\%$), (c) sample 10, $x = 0.55$ ($Mn^{4+} = 58.2\%$).

when the field is removed. This feature has been seen for other charge-ordered manganites (see for example [12, 20]).

In samples $4 \rightarrow 9$ at intermediate temperatures ($70\ \text{K} \lesssim T \lesssim 160$ K, depending on the sample), where the transport is dominated by the charge-ordered electrons even at $H \sim 9$ T, the magnetization rises sharply at $H < H_k$ and then increases gradually with field and exhibits little hysteresis, whereas the resistivity displays a strong hysteresis. The resistivity decreases smoothly with increasing field and does not display any abrupt jump as at low temperatures. On decreasing the field, however, $\rho(H)$ increases and first remains lower than in the initial sweep, but at lower fields ($H \lesssim 1$ T) it rises above initial sweep, so the resistivity at $H = 0$ is higher than in the initial ZFC sweep. This feature is also exhibited by sample 10, which remains activated down to the lowest temperatures [27] even at $H \sim 9$ T (see figure 9(c)), although not only does ρ cross over the initial sweep at a higher field ($H \lesssim 3$ T), but also the drop in ρ with field is not as sharp (as is demonstrated by the roundedness of the data). This

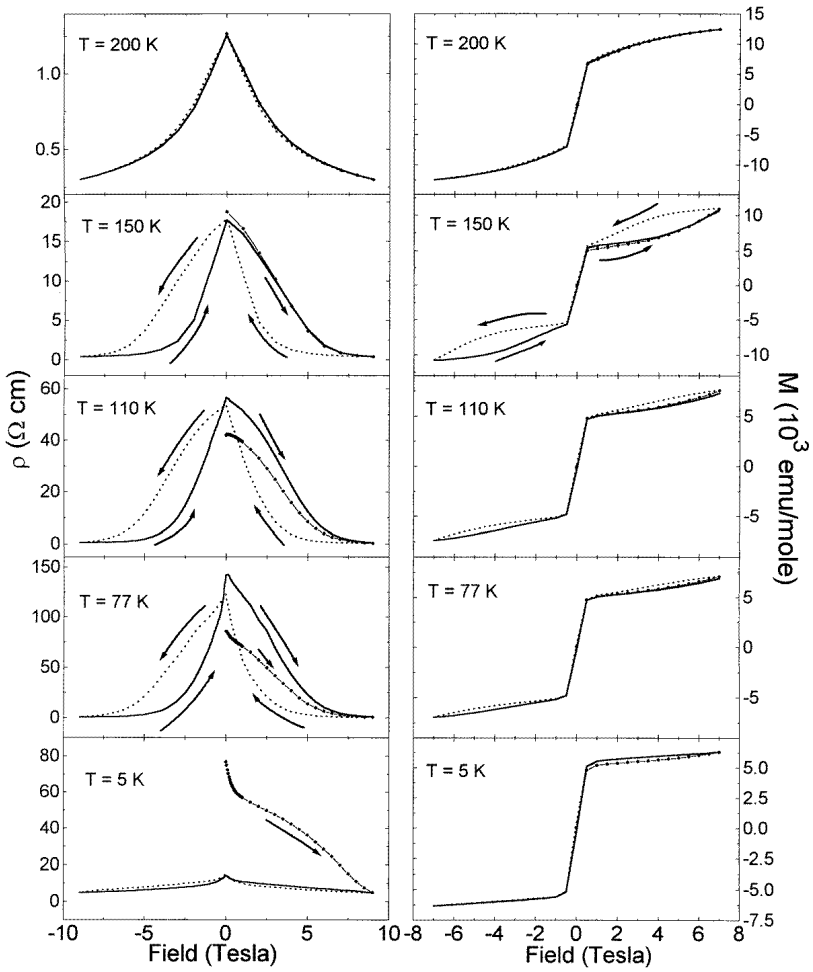

(b)

Figure 9. (Continued)

behaviour was also observed in data for high-quality samples of $Pr_{0.50}Sr_{0.50}MnO_3$ [19], and therefore appears to be intrinsic to some materials with $x \approx 0.50$. In fact, in the intermediate-temperature regime, ρ at low fields increases with subsequent field sweeps. We speculate that this increase in ρ at low fields is due to a field-induced '*annealing*' of the charge-ordered state; i.e. by sweeping the field up and back to zero, more perfect charge-ordered states with correspondingly higher resistivity are created.

For samples $4 \rightarrow 10$ near T_{co}, both $\rho(H)$ and $M(H)$ show hysteresis, although no difference between the initial sweep and the subsequent rise in the field after a complete magnetic field loop is displayed by either of them. At $T > T_{co}$, the magnetization increases sharply at $H < H_k$ with a corresponding relatively sharp drop in resistivity. But at a higher temperature ($T \gg T_{co}$), both $\rho(H)$ and $M(H)$ change gradually with field and neither of them displays any hysteresis. In fact, H_k decreases with increasing temperature and eventually becomes zero, which is illustrated by the typical paramagnetic characteristics of $M(H)$ and the roundedness of the resistivity data at low fields.

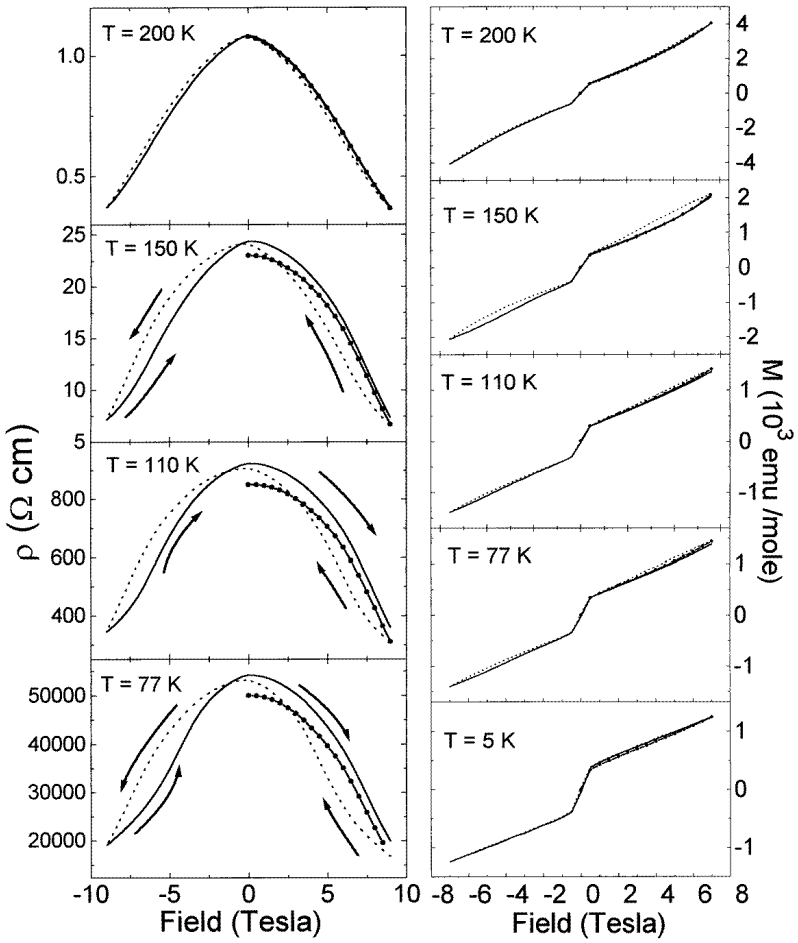

(c)

Figure 9. (Continued)

5. Conclusions

In conclusion, we have performed a careful study of the properties of $La_{1-x}Ca_xMnO_3$ in the regime near the doping-induced MIT ($x \sim 0.50$). We find that the properties are highly sensitive to both the exact Ca and Mn^{4+} contents. More importantly, we find that the electronic transport properties of these materials in this regime can be understood within a model of coexistence of free carriers and real-space charge ordering. On the basis of our data, the 'melting' of the charge order by application of a magnetic field appears to progress through an increase in the number of free carriers. Such a coexistence at exactly $x \approx 0.50$ has also been observed in recent TEM and optical work [28], and has also been suggested from Mössbauer [29] and NMR studies [30].

Our data suggest that the coexistence of charge order and free carriers persists to both lower and higher doping near $x \sim 0.50$, which implies that the properties of the materials even in the ferromagnetic regime at lower doping are probably affected by the presence of small regimes of phase-separated charge order. Indeed, such phase separation forms the basis for

recent theoretical efforts, which have been quite successful in describing these materials [31]. Future studies will include a more detailed examination of the properties of these materials across the MIT with better-controlled samples more finely spaced in doping and Mn^{4+} content.

Acknowledgments

This research was supported by NSF grant DMR 97-01548, the Alfred P Sloan Foundation and the Department of Energy, Basic Energy Sciences—Materials Sciences under contract No W-31-109-ENG-38.

References

[1] Tokura Y (ed) 1999 *Colossal Magnetoresistive Oxides* (New York: Gordon and Breach) at press
[2] Hwang H Y, Cheong S-W, Radaelli P G, Marezio M and Batlogg B 1995 *Phys. Rev. Lett.* **75** 914
Ogale S B, Talyansky V, Chen C H, Ramesh R, Greene R L and Venkatesan T 1996 *Phys. Rev. Lett.* **77** 1159
Zhou J-S, Goodenough J B, Asamitsu A and Tokura Y 1997 *Phys. Rev. Lett.* **79** 3234
Neumeier J J, Hundley M F, Thompson J D and Heffner R H 1995 *Phys. Rev.* B **52** R7006
Khazeni K, Jia Y X, Lu Li, Crespi V H, Cohen M L and Zettl A 1996 *Phys. Rev. Lett.* **76** 295
[3] Ramirez A P 1997 *J. Phys.: Condens. Matter* **9** 8171
[4] Jonker G H and Van Santen J H 1950 *Physica* **16** 337
Jonker G H and Van Santen J H 1950 *Physica* **16** 599
[5] Wollan E O and Koehler W C 1955 *Phys. Rev.* **100** 545
[6] Matsumoto G 1970 *J. Phys. Soc. Japan* **29** 606
Matsumoto G 1970 *J. Phys. Soc. Japan* **29** 615
[7] Schiffer P, Ramirez A P, Bao W and Cheong S-W 1995 *Phys. Rev. Lett.* **75** 3336
[8] Zener C 1951 *Phys. Rev.* **81** 440
Zener C 1951 *Phys. Rev.* **82** 403
Anderson P W and Hasegawa H 1955 *Phys. Rev.* **100** 675
de Gennes P G 1960 *Phys. Rev.* **118** 141
[9] Millis A J, Littlewood P B and Shraiman B I 1995 *Phys. Rev. Lett.* **74** 5144
Millis A J, Shraiman B I and Mueller R 1996 *Phys. Rev. Lett.* **77** 175
Millis A J 1996 *Phys. Rev.* B **53** 8434
Roder H, Zhang J and Bishop A R 1996 *Phys. Rev. Lett.* **76** 1356
Zhao G M, Conder K, Keller H and Muller K A 1996 *Nature* **381** 676
[10] Ramirez A P, Schiffer P, Cheong S-W, Chen C H, Bao W, Palstra T T M, Gammel P L, Bishop D J and Zegarski B 1996 *Phys. Rev. Lett.* **76** 3188
[11] Bao W, Axe J D, Chen C H and Cheong S-W 1997 *Phys. Rev. Lett.* **78** 543
[12] Xiao G, McNiff E J Jr, Gupta A, Canedy C L and Sun J Z 1996 *Phys. Rev.* B **54** 6073
These authors observed distinct steps in $\rho(H)$, which were not observed for any of our samples.
Xiao G, McNiff E J Jr, Gupta A, Canedy C L and Sun J Z 1997 *J. Appl. Phys.* **81** 5324
Gong G Q, Canedy C, Xiao G, Sun J Z, Gupta A and Gallagher W J 1995 *Appl. Phys. Lett.* **67** 1783
[13] Chen C H and Cheong S W 1996 *Phys. Rev. Lett.* **76** 4042
Liu K, Wu N W, Ahn K H, Sulchek T, Chein C L and Xiao J Q 1996 *Phys. Rev.* B **54** 3007
[14] Kawano H, Kajimoto R, Yoshizawa H, Tomioka Y, Kuwahara H and Tokura Y 1997 *Phys. Rev. Lett.* **78** 4253
[15] Papavassiliou G, Fardis M, Milia F, Simopoulos A, Kallias G, Pissas M, Niarchos D, Ioannidis N, Dimitropoulos C and Dolinsek J 1997 *Phys. Rev.* B **55** 15 000
[16] Radaelli P G, Cox D E, Marezio M, Cheong S-W, Schiffer P and Ramirez A P 1995 *Phys. Rev. Lett.* **75** 4488
Radaelli P G, Cox D E, Marezio M and Cheong S-W 1997 *Phys. Rev.* B **55** 3015
[17] Tomioka Y, Asamitsu A, Kuwahara H, Moritomo Y and Tokura Y 1996 *Phys. Rev.* B **53** R1689
Urushibara A, Moritomo Y, Arima T, Asamitsu A, Kido G and Tokura Y 1995 *Phys. Rev.* B **51** 14 103
[18] Roy M, Mitchell J F, Ramirez A P and Schiffer P 1998 *Phys. Rev.* B **58** 5185
[19] Tomioka Y, Asamitsu A, Moritomo Y, Kuwahara H and Tokura Y 1995 *Phys. Rev. Lett.* **74** 5108
[20] Tokura Y, Kuwahara H, Moritomo Y, Tomioka Y and Asamitsu A 1996 *Phys. Rev. Lett.* **76** 3184
Yoshizawa H, Kawano H, Tomioka Y and Tokura Y 1995 *Phys. Rev.* B **52** R13 145
[21] Jaime M, Salamon M B, Rubinstein M, Treece T E, Horwitz J S and Chrisey D B 1996 *Phys. Rev.* B **54** 11 914
Billinge S J L, DiFrancesco R G, Kwei G H, Neumeier J J and Thompson J D 1996 *Phys. Rev. Lett.* **77** 715

Palstra T T M, Ramirez A P, Cheong S-W, Schiffer P and Zaanen J 1997 *Phys. Rev.* B **56** 5104
Tyson T A, Mustre de Leon J, Conradson S D, Bishop A R, Neumeier J J, Roder H and Zhang Jun 1996 *Phys. Rev.* B **53** 13 985

[22] The error in the fit parameters (A, B, C, D) is within ∼30%.

[23] Mott N F 1974 *Metal–Insulator Transition* (London: Taylor and Francis)

[24] Ju H L, Gopalakrishnan J, Peng J L, Li Qi, Xiong G C, Venkatesan T and Greene R L 1995 *Phys. Rev.* B **51** 6143

[25] Kasai M, Kuwahara H, Tomioka Y and Tokura Y 1996 *J. Appl. Phys.* **80** 6894

[26] Hwang H Y, Cheong S-W, Ong N P and Batlogg B 1996 *Phys. Rev. Lett.* **77** 2041

[27] The resistivity at $T \sim 5$ K is beyond the range of our resistance bridge.

[28] Calvani P, De Marzzi G, Dore P, Lupi S, Maselli P, D'Amore F and Gagliardi S 1998 *Phys. Rev. Lett.* **81** 4504
Mori S, Chen C H and Cheong S-W 1998 *Phys. Rev. Lett.* **81** 3972 and references therein

[29] Kallias G, Pissas M, Devlin E, Simopoulos A and Niarchos D 1999 *Phys. Rev.* B **59** 1272

[30] Allodi G, De Renzi R, Licci F and Pieper M W 1998 *Phys. Rev. Lett.* **81** 4736

[31] Yunoki S, Hu J, Malvezzi A L, Moreo A, Furukawa N and Dagotto E 1998 *Phys. Rev. Lett.* **80** 845
Moreo A, Yunoki S and Dagotto E 1999 *Science* **283** 2034